An Overview of Voltage Boosting Techniques and Step-Up DC-DC Converters Topologies for PV Applications

Márcio R. S. de Carvalho [ID]**, Rafael C. Neto** [ID]**, Eduardo J. Barbosa** [ID]**, Leonardo R. Limongi** [ID]**, Fabrício Bradaschia** [ID] **and Marcelo C. Cavalcanti** *[ID]

Power Electronics and Drives Research Group (GEPAE), DEE, Universidade Federal de Pernambuco, Recife 50740-530, Brazil; marcio.rodrigosantos@ufpe.br (M.R.S.d.C.); rafael.cavalcantineto@ufpe.br (R.C.N.); eduardo.josebarbosa@ufpe.br (E.J.B.); leonardo.limongi@ufpe.br (L.R.L.); fabricio.bradaschia@ufpe.br (F.B.)
* Correspondence: marcelo.ccavalcanti@ufpe.br

Abstract: The development of technologies to improve the performance of photovoltaic (PV) module integrated converters (MICs) is fundamental to increase the use of distributed generation systems with photovoltaic power source in large urban centers, mainly for complex residential roofs. For two-stage PV MICs, high step-up DC-DC converters are required to boost the low PV module voltage to a higher voltage, in order to suit the DC bus voltage requirements of grid-tied inverters. Thus, to support researchers interested in developing DC-DC power conversion for PV microinverters, this paper classifies the DC-DC converters according to their operational and constructive characteristics and presents some elementary voltage-boosting techniques to aid in analyzing and understanding more complex topologies. Finally, high step-up DC-DC converters based on magnetic coupling and switched capacitor widely cited by important works related to PV applications are presented, with their principles of operation analysed in a simple and objective way, but sufficient to understand their capability to provide high voltage gain. The approach presented by this paper leads to insight into how to place the energy storage elements to create new topologies of DC-DC converters, so that high voltage gain is achieved, and how to analise the high voltage gain capability of complex topologies

Keywords: categories of DC-DC converters; high step-up DC-DC converters; microinverter; voltage-boosting techniques; voltage multiplier cell

1. Introduction

In recent years, the deployment of grid-connected photovoltaic (PV) system in large urban centers has increased significantly thanks to cost reductions and technological advances in PV module integrated converters (MICs), intended to perform maximum power point tracking (MPPT) per PV module [1]. Such feature, known as distributed MPPT, mitigates the power losses caused by PV module mismatch (e.g., manufacturing tolerance) [2] and enables the installation of PV panel on rooftop with different tilts and orientations, susceptible to partial shading caused by neighbouring buildings [3].

MICs can have either single-stage or two-stages conversion systems: single-stage MICs perform voltage boosting, MPPT and grid current control in a single DC-AC power conversion; two-stages MICs have a DC-DC stage to boost the PV module DC voltage (between 20 V–45 V) to a higher value (above 380 V, for instance) while tracking the PV module maximum power point, followed by a DC-AC stage, responsible to DC-link voltage regulation and the grid-tied functions [4]. The main drawback of single-stage MICs is that the double-line-frequency voltage ripples must be filtered by a bulky input electrolytic capacitors at the input side [5], which affects the stable implementation of MPPT algorithms and reducing the life span of the entire system whereas two-stages MICs employ proper control strategies alongside small electrolytic capacitors in both conversion stages to eliminate it [6].

Compared to architectures with central inverter, MICs are inherently safer because the DC energy is converted to AC right at the site of the PV module [7]. Hence, they operate at the same low-voltage AC power as the grid utility, which means there is no long-distance high voltage DC cables [4]. Besides, since MICs are mounted in a single PV module and operate independently, system with MICs keeps delivering energy to the grid if one or more MICs fail while if a system with a central inverter fails, the energy production stops completely. Moreover, MICs allow simultaneously usage of different solar panels technology and faster and easier system expansion, possibly at any time, thanks to their plug-and-play technology [5].

Due to above-mentioned advantages provided for MICs, several high step-up DC-DC converters have been proposed in the literature for being employed as DC-DC power conversion stage in MICs. However, some of them do not meet the other necessary requirements such as high-efficiency, common ground, low input current ripple and reduced weight and volume. Thus, to assist researchers in developing module-level power electronics, this paper categorizes the DC-DC converters based on their constructive and operational characteristics. Then, the principles of elementary voltage-boosting techniques such as switched-capacitor, switched-inductor, magnetic coupling and voltage multiplier cells are approached, with their advantages and disadvantages stated.

Throughout this paper, some high step-up DC-DC converters based on switched capacitor and magnetic coupling already published in the literature and widley cited by important papers in the field of PV MICs are presented and discussed in such a way that their operation stages related to the process of charging and discharging of the energy stored elements are quite explored, highlighting the components of the power branch. During the description of this stages, the voltages across the capacitors and magnetic elements are determined to facilitate understanding how high voltage gain is achieved. This approach allows researchers to gain the insight needed to develop high step-up DC-DC converters and to effectively analise more complex topologies in order to understand their capacity to provide high voltage gain. To the best of the authors' knowledge, this methodology is an original contributions of the present paper. Finally, for each converter described, its main features in regard to the desirable characteristics in PV MICs are summarized.

2. Categories of Step-Up DC-DC Converters

The DC-DC converters topologies proposed in the literature can be categorized according to their operational characteristics. Doing so, it becomes possible to evaluate which characteristics the step-up DC-DC converters intended for PV applications must feature. For this purpose, DC-DC converters can be essentially classified as (Figure 1): isolated or non-isolated; unidirectional or bidirectional; current- or voltage-fed; and hard- or soft-switched.
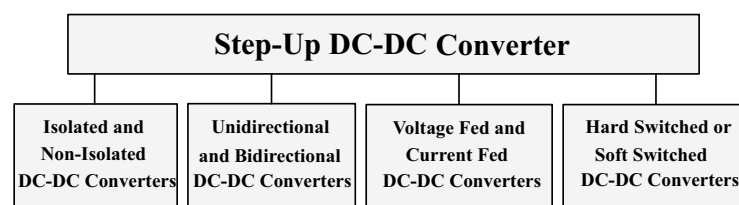

Figure 1. Categories of step-up DC-DC converters.

2.1. Isolated and Non-Isolated DC-DC Converters

Regarding the presence of galvanic isolation, DC-DC converters can be classified into isolated or non-isolated. The isolated converters are characterized for using transformers to obtain the desired voltage gain. However, the leakage inductance of the transformer windings leads to high voltage spikes on the main switch and, consequently, high switching losses.

In applications that do not demand high voltage gain or high efficiency, non-isolated converters without magnetic coupling can be a simple (since the design of the magnetic element is eliminated) and adequate solution.

There are also non-isolated DC-DC converters that use built-in transformer and/or coupled inductor. These solutions are suitable candidates to be employed in applications where high voltage gain with high efficiency and reliability are required, such as microinverters and power optimizers.

In both types of non-isolated DC-DC converters (with or without magnetic coupling), the negative terminal of the output voltage can either be connected to the negative terminal of the input voltage or be floating. However, in grid-connected PV applications where galvanic isolation is not mandatory, the first option can be used to improve system performance. In fact, it helps to reduce the leakage currents between the converter and the point of common coupling, which is grounded.

2.2. Unidirectional and Bidirectional DC-DC Converters

In most DC-DC converters, the power flow is unidirectional (from input to output). This feature is required in applications where the input source should only supply power to the load, e.g., PV modules. On the other hand, in applications that have energy storage systems, DC-DC converters with the ability to transfer energy bidirectionally must be used.

2.3. Voltage- and Current-Fed DC-DC Converters

With respect to the input filter, DC-DC converters can be classified into voltage- or current-fed. The first configuration is characterized for having a capacitive input filter while the second one has an inductive input filter. The use of an inductive input filter makes possible to attenuate the input current ripple, which is a desired feature to step-up DC-DC converters that are used in PV MICs. Furthermore, both configurations can operate with soft switching in applications with variable input voltage. Due to the characteristics described above, the current-fed DC-DC converters are very popular in PV applications, as PV modules behave as current sources.

2.4. Hard- or Soft-Switched DC-DC Converters

The DC-DC converters can operate with hard- or soft-switching. In hard-switched DC-DC converters, the currents and voltages on the semiconductors during the turn-on and turn-off transitions are different from zero, causing switching losses. For this reason, the switching frequency in these converters must be limited, which commits the goals of minimizing the size of the energy storage elements. Besides, these converters are affected by electromagnetic interference problems due to the high current and voltage variation rates.

In soft-switched DC-DC converters, the voltage on the switches falls to zero and, immediately after a short time interval—called dead time—the switches are turned on, mechanism known as "zero voltage switching" (ZVS). Furthermore, small capacitors can be added in series with the leakage inductance of the magnetic element to form resonant operation stages. In these stages, the current flowing through the diodes decreases naturally to zero before the diode becomes reverse-biased, mechanism known as "zero current switching" (ZCS).

2.5. Usual Requirements of DC-DC Converters for Microinverters

From the evaluation of the operational characteristics presented in this section, the main requirements that DC-DC converters intended for PV microinverters should meet are:

(i)   Common ground, i.e., the DC-DC converter must be non-isolated;
(ii)   High voltage gain capability, i.e., the DC-DC converter must be a step-up converter; and
(iii)   unidirectional.

It is important to point out that soft switching and resonant mechanisms can lead to reduced switching loss, which is desirable in PV microinverters.

As indicated in the requirements described above, step-up DC-DC converters are the most commonly used solution for DC-DC power conversion stage in MICs. The most common converter that belongs to this category is the conventional boost converter. However, it has several drawbacks already observed in the literature, such as its non-capability to provide high voltage gain. Thus, before presenting some step-up DC-DC converters proposed in the literature for PV applications, it is extremely important to understand how basic voltage-boosting techniques work.

3. Voltage-Boosting Techniques

Since two-stage PV microinverters require high step-up DC-DC converters to boost the PV module low DC voltage, it is important to review the main voltage-boosting techniques presented in the literature [8]: switched capacitor; switched inductor and voltage lift; magnetic coupling; and voltage multiplying cells. Essentially, these techniques use energy storage elements (inductors and capacitors) and/or transformers among with switches and diodes to create step-up cells that have higher voltage gain and efficiency than the classic boost converter (without its limitations).

3.1. Switched Capacitor

The switched capacitor technique can be easily understood by analysing the two operating stages of the basic voltage-doubler, which is shown in Figure 2. During the stage shown in Figure 2a, the capacitor C_1 is charged by the input voltage source (V_{in}). During the complementary stage, shown in Figure 2b, the capacitor C_1 is discharged in series with the input source. As result of this operation, the output voltage is twice the input voltage, justifying the name of the topology.
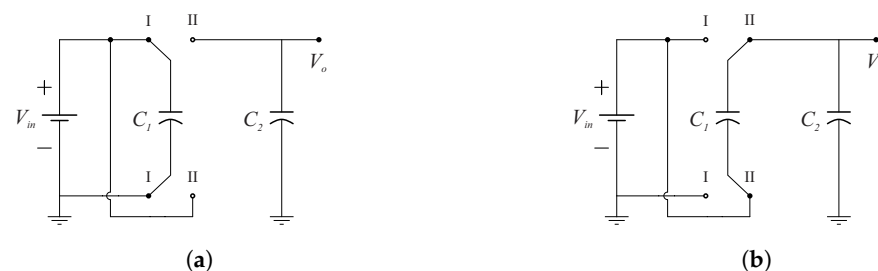

Figure 2. Operation stages of the voltage-doubler based on the switched capacitor technique [8]. (**a**) Stage 1. (**b**) Stage 2.

From the topology presented above, it can be pointed out that the basic voltage-doubler cell based on switched-capacitor is comprised of one capacitor; and four semiconductors, which operate in a complementary way. In this cell, the energy is transferred from input to output by charging and discharging the capacitors in parallel and series, respectively. Thus, high voltage gains can be achieved by connecting many of these cells in cascade [9]. For example, the circuit shown in Figure 3 is formed by the cascade connection of two voltage-doublers. In this case, the output voltage of each stage is twice its input voltage, that is, $V_{C_2} = 2 \cdot V_{in}$ and $V_{C_4} = 2 \cdot V_{C_2} = 4 \cdot V_{in}$.
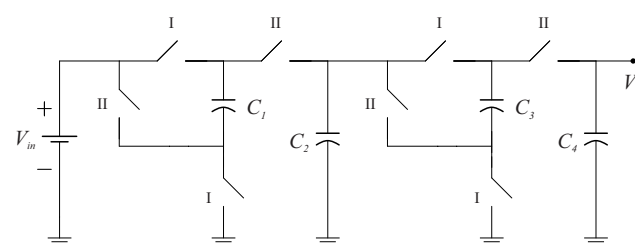

Figure 3. Circuit formed by voltage-doublers connected in series [8,9].

However, due to the requirements for high voltage gain, more switching capacitor stages are needed. This makes the final circuit complex for voltages gains greater the 15, with a large number of components. Another disadvantage of this technique is that, as the capacitors terminals are series-connected, it is hard to guarantee the voltage balance between the capacitors. On the other hand, as there are no magnetic elements, the size and weight of the final circuit and the voltage stresses on the switches are reduced [10].

3.2. Switched Inductor and Voltage Lift

The switched inductor technique can be easily understood by analysing the operating stages of the circuit shown in Figure 4, which consist of the conventional boost converter with a basic switched inductor cell. In the first operation stage (Figure 4a), the inductors are connected in parallel and charged by the input power source with voltage V_{in}. In the complementary stage, shown in Figure 4b, the inductors are connected in series and discharged with voltage $\frac{D}{1-D}V_{in}$. Therefore, the power branch contains, associated in series (i.e., with the voltages added), the input voltage source and the two inductors (L_1 and L_2). Thus, the voltage across the output capacitor is given by:

$$V_C = \frac{1+D}{1-D} \cdot V_{in}. \tag{1}$$

In order to obtain higher voltage gains, the basic switched inductor cell (second column of Table 1) can be integrated with the elementary voltage-lift cell (Figure 5), which replaces L_1, resulting in the well-known self-lift switched inductor cell, which is shown in third column of Table 1. Adding one diode and one capacitor to this cell, the double self-lift switched inductor cell is obtained, which is shown in the fourth column of Table 1.

Usually, the voltage lift cells shown in Table 1 are inserted before the main switch of the conventional boost converter, as shown in Figure 4. Therefore, the voltage stress on the switch is equivalent to the voltage between the output terminals of the converter. Because of this characteristic, converters based on this technique must, necessarily, use switches with high breakdown voltage and, thus, with high on-resistance. Consequently, the conduction losses in the main switch are quite significant.
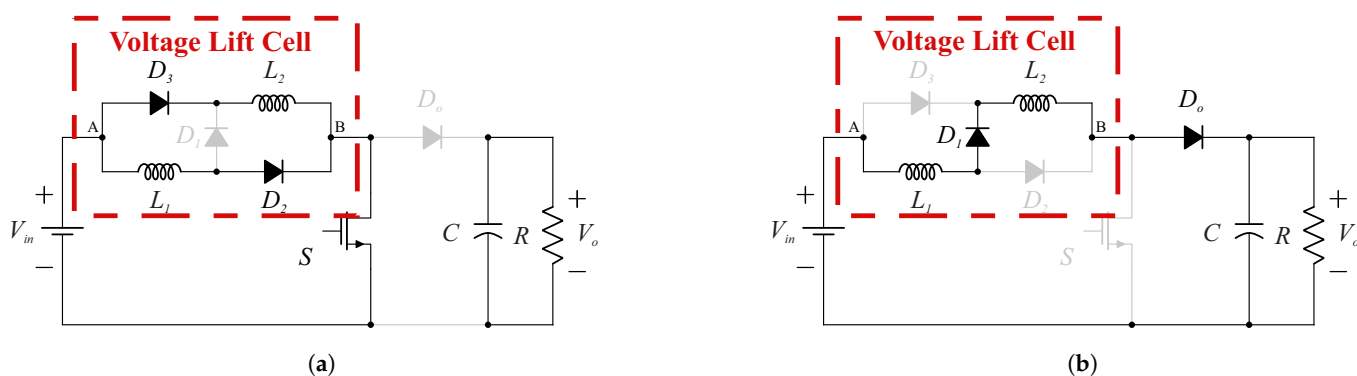

(**a**)　　　　　　　　　　　　　　　　　　　　　　　　　(**b**)

Figure 4. Operation stages of a boost converter with a basic switched inductor cell. (**a**) Stage 1—the switch is conducting. (**b**) Stage 2—the switch is blocking current circulation.
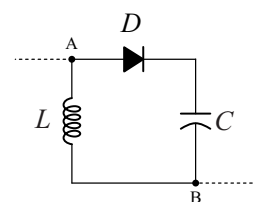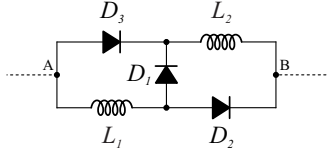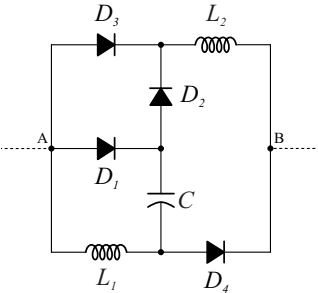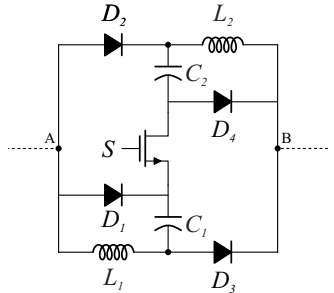

Figure 5. Elementary voltage-lift cell.

Table 1. Comparison between different voltage lift switched inductor cells [8,11].

Voltage Lift Cell	Basic Switched Inductor [12]	Self-Lift Switched Inductor Cell [11]	Double Self-Lift Switched Inductor Cell [11]
Circuit			
Voltage Gain	$\dfrac{1+D}{1-D}$	$\dfrac{2}{1-D}$	$\dfrac{3-D}{1-D}$
Number of Passive Elements	0 capacitors 2 inductors	1 capacitor 2 inductors	2 capacitors 2 inductors
Number of Semiconductors	0 switches 3 diodes	0 switches 4 diodes	1 switch 4 diodes

Another relevant solution based on switched inductor technique is the active switched inductor based converter [13], shown in Figure 6, which operates similarly to the converter in Figure 4, but with power flow controlled by switches instead of diodes. Since both switches are turned on and turned off synchronously, under the same experimental conditions, the voltage stresses on the switches of the active switched inductor based converter are lower than the voltage stress on the switch of the boost converter with a basic switched inductor cell by a reduced factor of ($\frac{D}{1-D}V_{in}$ − inductor discharge voltage). However, in general, the reference terminals of the input and output voltages of the active switched inductor based converter are not connected [14]. Other examples of converters based on active switched inductors network can be found in [15,16].
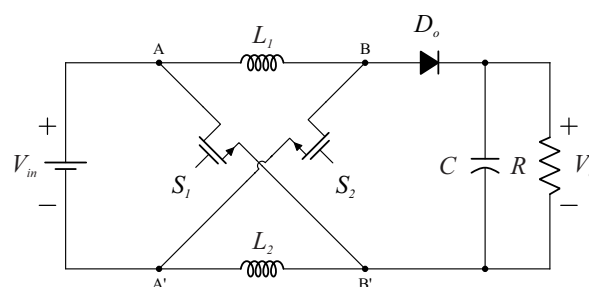
Figure 6. Active switched inductor based converter.

Finally, it must be highlighted that active switched inductors networks differ from switched inductors cells, because the networks incorporate the switches of the converter, while cells do not [16].

3.3. Magnetic Coupling

Magnetic coupling technique is widely used in DC-DC converters, isolated or non-isolated, through use of transformers and/or coupled inductors to obtain high voltage

gains. Naturally, there is a reduction in cost and volume when using magnetically coupled windings on a single core instead of, for example, two simple inductors.

Although superficially similar, transformers and coupled inductors are different in constructive and operational aspects. Coupled inductors are devices used primarily to store energy during part of the switching cycle, and release all of their stored energy in the complementary stage, while transformers are devices used to transfer power, scaling via their turns ratio the currents and voltages, and to provide galvanic isolation between the inputs and outputs. Consequently, in coupled inductors, unlike transformers, the instantaneous input power is not equal to the instantaneous output power. Also, due to the energy storage requirement, coupled inductors employ gaps [17], while transformers does not.

Another important difference between these magnetic elements is that the current conversion ratio in coupled inductors is determined by the circuit within which they are inserted. Thus, the energy stored in the inductor is adjusted to maintain the currents required by the circuit. On the other hand, in transformers, this relation is defined exclusively by the designed transformer turn ratio [18].

3.4. Voltage Multiplier Cells

Voltage multiplier cells (VMCs) are structures that use the switched capacitor technique, with or without additional magnetic elements, in the converter (usually after the main switch in order to reduce voltage stress on it) to raise the output voltage. VMCs composed only of diodes and capacitors are known as switched capacitor VMCs [19]. Inductors can also be added to the VMC to provide ZCS at the turn-off transition of the diodes and/or to raise the voltage gain. The representation of the boost converter with VMC is shown in Figure 7. Examples of classic VMCs are shown in Figure 8.
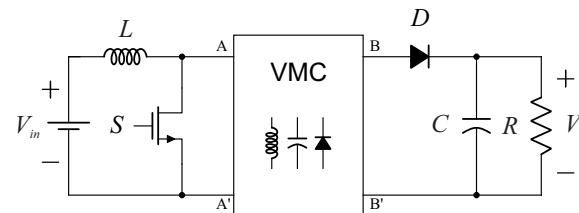

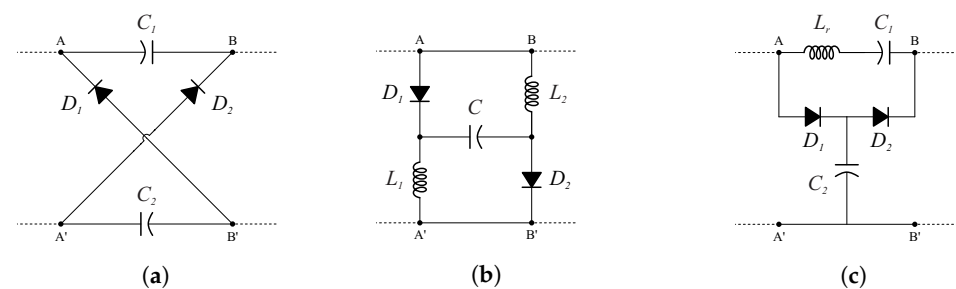**Figure 7.** Boost converter with VMC [19].

Figure 8. Classic VMCs. (**a**) Switched/diode capacitor VMC [20]. (**b**) VMC with capacitor, diode and inductor [21]. (**c**) VMC with resonant inductor [22].

There are also DC-DC converters based on VMCs with coupled inductor and/or non-isolated transformers. In these converters, the primary winding of the magnetic element is connected directly (or through diodes and capacitors) to the main switch, while the secondary winding (together with diodes and capacitors) compose the VMC, which is inserted in one of the following positions: (i) between the primary winding and the converter output (horizontal structure shown in Figure 9a); or (ii) above the primary winding (vertical structure shown in Figure 9b) [8]. In addition, it is possible to incorporate a clamp snubber circuit in the VMCs to limit the voltage stress on the main switch caused by leakage inductances of magnetic elements.
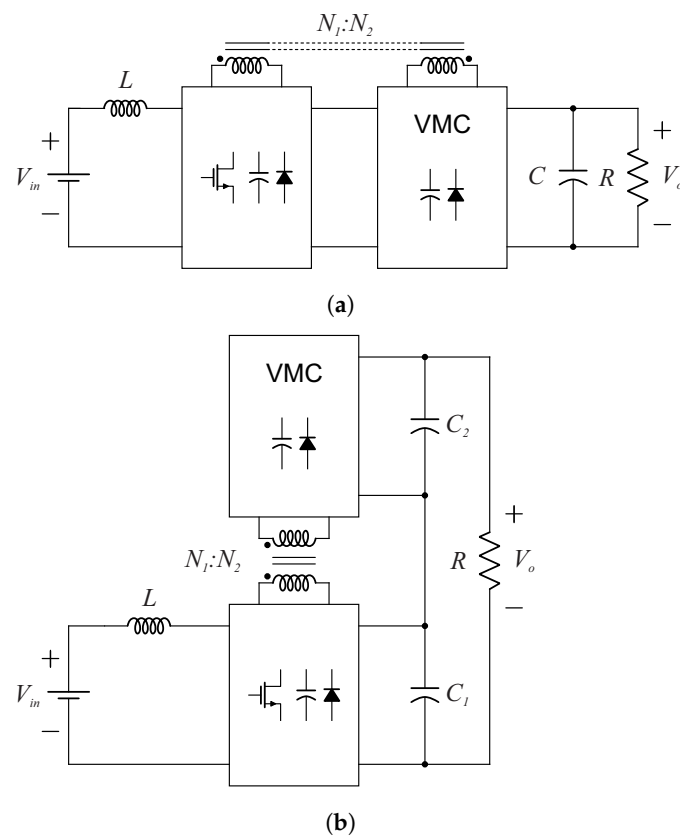
Figure 9. General structures of VMCs with magnetic coupling. (**a**) Horizontal structure. (**b**) Vertical structure.

Doing so, it becomes possible to integrate the positive aspects of different voltage-boosting techniques and clamp circuits. This versatility, together with the low complexity of VMCs, makes them useful in DC-DC converters intended for use in application where the requirements go beyond the needed high voltage gain.

4. Recent Advances on DC-DC Converters for Microinverters

In this section, some non-isolated DC-DC converters based on coupled inductor (or built-in transformer) and switched capacitor techniques proposed in the literature and widely cited by important papers in the field of PV microinverters are listed and discussed, with emphasis on the operation stages in which the energy storage elements are charged and discharged to transfer power to the load. Then, a brief comparison between them is presented as well.

4.1. DC-DC Converter with Built-In Transformer Voltage Multiplier Cell Proposed

The DC-DC converter proposed in [23], shown in Figure 10, uses a VMC combined with magnetic coupling (built-in transformer) and switched capacitor techniques, and clamp circuit to limit the voltage stress on the switch. In this converter, the turns ratio of the built-in transformer is designed for, together with the duty cycle (D), obtaining high voltage gain at the output terminals.

Depending on the ratio between the time interval in which the switch conducts and the resonance period, this converter can operate in two different modes: over resonant frequency (ORF); or below resonant frequency (BRF). In the first mode, the time interval in which the switch conducts (DT_s) is greater than the resonance period caused by the leakage inductance, L_{lk}, and the blocking capacitor, C_b. In the second, DT_s is less than the resonance period caused by associating L_{lk} and C_b in series.
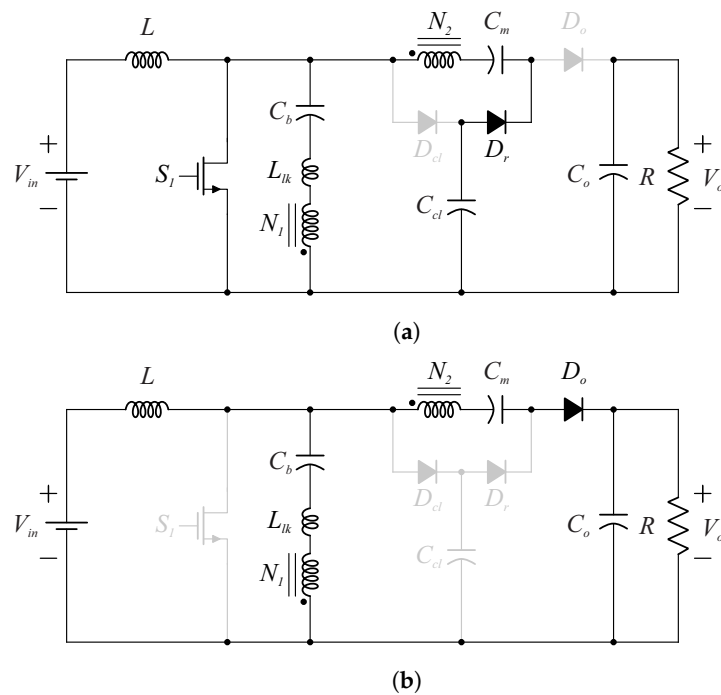
(a)

(b)

Figure 10. Main operation stages of the DC-DC converter proposed in [23]. (**a**) Operation stage that corresponds to the interval $[t_0 - t_1]$ of [23] (stage 1 of 5). (**b**) Operation stage that corresponds to the interval $[t_3 - t_4]$ of [23] (stage 4 of 5).

In a switching cycle, this converter presents five different operation stages. However, the operation stages shown in Figure 10a,b (common to ORF and BRF modes) are sufficient to observe the energy storage elements being charged and the power branch. By evaluating these stages, the following characteristics are observed:

- During the operation stage presented in Figure 10a, the input inductor is charged by the input voltage and the energy stored in the clamp capacitor (C_{cl}) is transferred to the switched capacitor (C_m) through the regenerative diode (D_r). In this circuit, there is resonance between the capacitor C_b and the leakage inductance L_{lk};
- During the operation stage presented in Figure 10b, the output diode conducts. At this moment, the voltage across the primary winding (N_1) is equal to the difference between the voltages over the clamp capacitor ($V_{cl} = \frac{V_{in}}{1-D}$) and blocking capacitor ($V_b = V_{in}$). Consequently, the voltage across N_2 is given by the following equation:

$$V_{N_2} = \left(\frac{N_2}{N_1}\right)\frac{D}{1-D}V_{in}. \tag{2}$$

The power branch contains the following components associated in series: (i) the input source; (ii) the input inductor; (iii) the switched capacitor; and (iv) high voltage winding of the transformer.

It must be pointed out that the operation stage shown in Figure 10b ends up when the resonant current flowing through the loop that contains the regenerative diode decreases to zero. Except for the output diode, the other diodes in this topology also turn off with zero-currents (non-resonant). Thus, there are no losses caused by the reverse recovery of the diodes. In addition, the voltage stress on the switch is equal to the output voltage of the classic boost converter, that is, $\frac{V_{in}}{1-D}$. This characteristic can be observed by analysing the position of the input voltage and the components L, S_1, D_{cl} and C_{cl} in the topology.

In summary, the main features of this converter are: (i) ZCS of the diodes; (ii) Hard switching at the turn-on and turn-off transition of the switch; (iii) common ground; (iv) low input current ripple; and (v) it employs one switch and two magnetic cores.

4.2. DC-DC Converter with Quasi-Resonant Operation Proposed

Forouzesh et al. [24] proposed a DC-DC converter with VMC in a vertical structure, shown in Figure 11. The VMC used in this topology is comprise of coupled inductor and switched capacitor, as the one presented in the previous subsection. In this converter, the voltage stress on the switch is limited by the clamp circuit formed, not explicitly, by the diode D_1 and the capacitor C_1. However, in this topology the VMC is placed above the boost converter with resonant loop. Then, when compared to the converter presented in the previous subsection, the topology proposed in [24] offers a higher voltage gain at the expense of using an additional diode and capacitor.
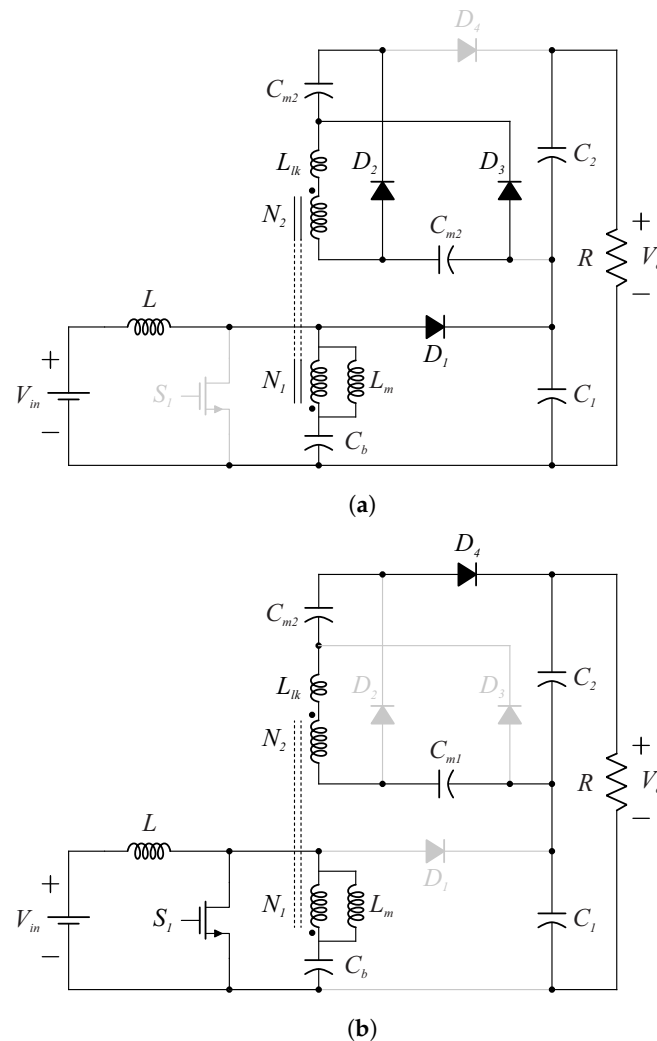
(a)

(b)

Figure 11. Main operation stages of the DC-DC converter proposed in [24]. (**a**) Operation stage that corresponds to the interval $[t_4 - t_0]$ of [24] (stage 5 of 5). (**b**) Operation stage that corresponds to the interval $[t_1 - t_2]$ of [24] (stage 2 of 5).

In a switching cycle, this topology presents five different operation stages. However, the operation stages shown in Figure 11a,b are enough to analyse the energy storage elements being charged and the power branch. Therefore, when analysing these stages, the following characteristics are observed:

- During the operation stage presented in Figure 11a, the switch and diode D_4 are turned-off. The coupled inductor is discharged with a voltage equal to $\frac{D}{1-D}V_{in}$. This energy is transferred to the switched capacitors, C_{m1} and C_{m2}, through the secondary winding (using the magnetic coupling). Thus, both switched capacitors are charged with voltage $V_{C_{m1}} = V_{C_{m2}} = \frac{N_2}{N_1}\frac{D}{1-D}V_{in}$;

- During the operation stage presented in Figure 11b, the diode D_4 and the switch (S_1) are conducting. The input voltage source V_{in} charges both the input and the coupled inductors. There is resonance between the blocking capacitor (C_b) and the leakage inductance of the primary winding (it is reflected for the secondary winding in Figure 11). The power branch contains, associated in series, the following components: (i) the capacitor C_1 ($V_{C_1} = \frac{1}{1-D}V_{in}$); (ii) the secondary winding of the coupled inductor ($V_{N_2} = \frac{N_2}{N_1}V_{in}$ in this operation stage); and (iii) the two switched capacitors.

It should be noted that the operation stage shown in Figure 11b ends up when the resonant current flowing through the diode D_4 decreases to zero. Although the operation stage in which D_1 conducts is not shown in Figure 11, in [24], it indicates that the current flowing through the diode D_1 (non-resonant) also decreases to zero before it becomes reverse-biased. Furthermore, the switching losses caused by the reverse recovery of diodes D_2 and D_3 are mitigated due to the leakage inductances of the coupled inductor, which control the rate at which the current flowing through them decreases during their turn-off transition.

The main features of this converter are: (i) Hard switching at the turn-on and turn-off transition of the switch; (ii) only two diodes with ZCS operation; (iii) low input current ripple; (iv) common ground; and (v) it employs one switch and two magnetic cores.

4.3. DC-DC Converter with an Asymmetric Voltage Multiplier Network Proposed

The DC-DC converter proposed in [25] employs a VMC derived from the combination of the elementary voltage-lift cell (Figure 5) with additional diode and capacitor. The derivation steps of the VMC are illustrated in Figure 12. Initially, the voltage-lift cell shown in Figure 12a is transformed into a voltage multiplier cell. Then, a clamp circuit formed by the capacitor C_b and the diode D_b is added to reduce the voltage stress on the main switch caused by the leakage inductance of the coupled inductor. Finally, the resulting VMC, which is based on switched capacitor and coupled inductor, is inserted into the conventional boost converter in order to obtain high voltage gain.
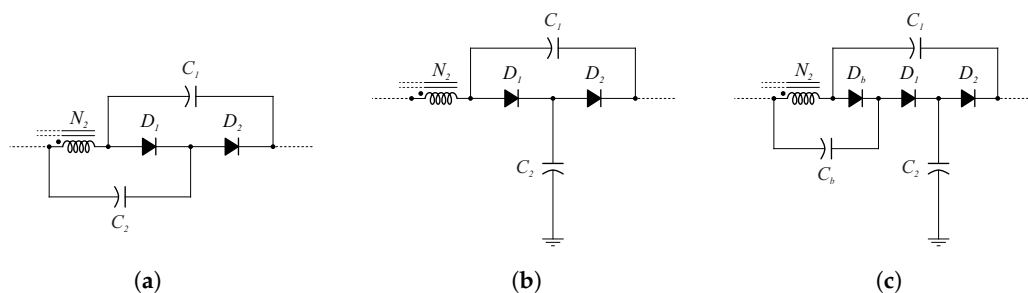

(a)   (b)   (c)

Figure 12. Development steps of the VMC presented in [25]. (**a**) STEP 1: Elementary voltage-lift celll with additional diode and capacitor. (**b**) STEP 2: Basic VMC. (**c**) STEP 3: VMC with clamp circuit.

In a switching cycle, the converter presents five different operation stages. Nevertheless, as done for the previous topologies, only two of these operation stages are approached (Figure 13a,b) since they are sufficient to observe the energy storage elements being charged and to understand the power branch. Thus, from this analysis, the following characteristics are observed:

- During the operation stage presented in Figure 13a, the coupled inductor is charged by the input voltage while the energy stored in the clamp capacitor (C_{cl}) is transferred to the switched capacitor (C_m) through the regenerative diode D_r;
- During the operation stage presented in Figure 13b, the output diode conducts (D_o). At this moment, the voltage across the primary winding N_1 is equal to $\frac{D}{1-D}V_{in}$. Consequently, the voltage across N_2 is given by:

$$V_{N_2} = \frac{N_2}{N_1}\frac{D}{1-D}V_{in}. \tag{3}$$

The power branch contains, associated in series, the following components: (i) the input voltage source; (ii) both windings of the coupled inductor; and (iii) the switched capacitor.
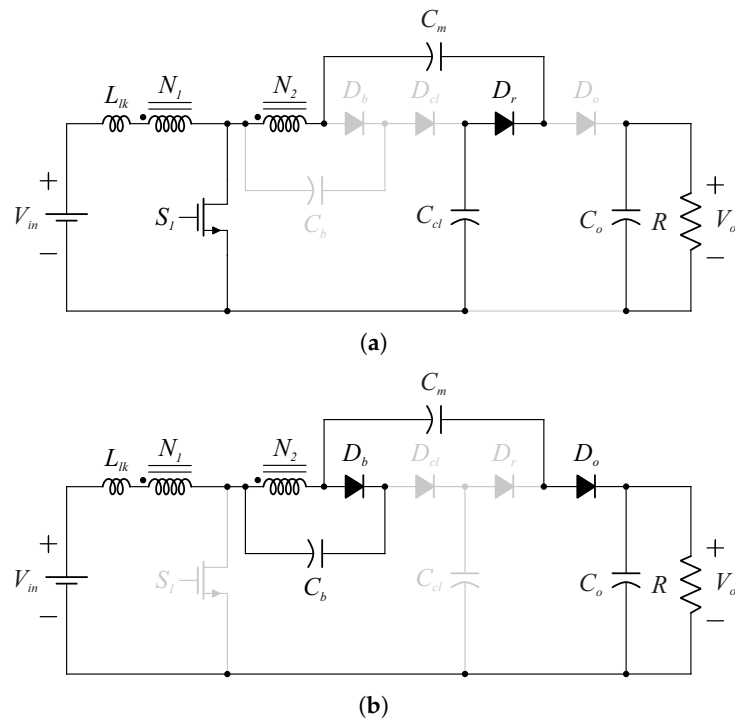

Figure 13. Main operation stages of the DC-DC converter proposed in [25]. (**a**) Operation stage that corresponds to the interval $[t_1 - t_2]$ of [25] (stage 2 of 5). (**b**) Operation stage that corresponds to the interval $[t_4 - t_5]$ of [25] (stage 5 of 5).

Although not included in Figure 13, this converter has a short operation interval that occurs when the switch is not conducting, in which the capacitor C_{cl} is charged with high voltage due to the series association of the input voltage source (with voltage V_{in}), primary winding of the coupled inductor (with voltage $\frac{D}{1-D}V_{in}$) and capacitor C_b (whose voltage is equals to the one across the secondary winding of the coupled inductor, that is, $\frac{N_2}{N_1}\frac{D}{1-D}V_{in}$). Thus, it results in:

$$V_{C_{cl}} = \frac{1 + \frac{N_2}{N_1}D}{1-D} V_{in}. \tag{4}$$

As shown in Figure 13a, C_{cl} is associated in series with the secondary winding of the coupled inductor, charging the capacitor C_m with the voltage $\frac{(1+2nD)}{1-D}V_{in}$. For this reason, the gain of this converter is quite high. In addition, there is resonant loop formed by C_b and C_{cl}, ZCS of the diodes D_b, D_{cl} and D_r is achieved. The switching losses caused by the reverse recovery of the output diode, D_o, is attenuated by the leakage inductance of the coupled inductor.

Besides the characteristics described above, it is important to point out the following features of the DC-DC converter proposed in [25]: (i) very high input current ripple; (ii) hard switching at the turn-on and turn-off transition of the switch; (iii) common ground; and (iv) it employs one switch and one magnetic core.

4.4. DC-DC Converter with an Integrated Coupled Inductor Proposed

The converter presented in [26] employs VMC technique based on switched capacitor and magnetic coupling. In this proposal, there are two coupled inductors mounted on a single magnetic core, with three windings (N_1, N_2 and N_3). Thus, it optimizes the magnetic design and the number of components.

The windings N_1 and N_2 are connected as an autotransformer to increase the voltage gain, which also allows to reduce the total number of turns and, consequently, the volume and losses of the magnetic element. There is also magnetic coupling between the windings N_1 and N_3, which integrate the normal coupled inductor (not connected as an autotransformer).

In this topology, the desired voltage gain can be obtained by choosing the appropriate turns ratio $\frac{N_2}{N_1}$ and $\frac{N_3}{N_1}$, and the duty cycle D. As consequence, the magnetic element can be designed considering the reduction of current stresses on the switch, which implies lower conduction losses.

In a switching cycle, the DC-DC converter proposed in [26] presents three different operation stages. However, the stages shown in Figure 14a,b are sufficient to observe the energy storage elements being charged and the power branch. When evaluating these stages, one can observe that:

- During the operation stage shown in Figure 14a, the coupled inductor is charged by the input voltage source. The capacitor C_m is charged with a voltage equal to the difference between the sum of the voltages across the three windings and the output capacitor C_o, and the voltage across the capacitor C_{cl};
- During the operation stage presented in Figure 14b, the output diode (D_o) conducts. At this moment, the voltage across the primary winding (N_1) is equal to $\frac{D}{1-D}V_{in}$. Consequently, the voltage across N_2 is given by:

$$V_{N_2} = \frac{N_2}{N_1}\frac{D}{1-D}V_{in}. \tag{5}$$

Besides, the power branch contains, associated in series, the following components: (i) the input voltage source; (ii) two windings of the coupled inductor, connected as autotransformer; and (iii) the switched capacitor.
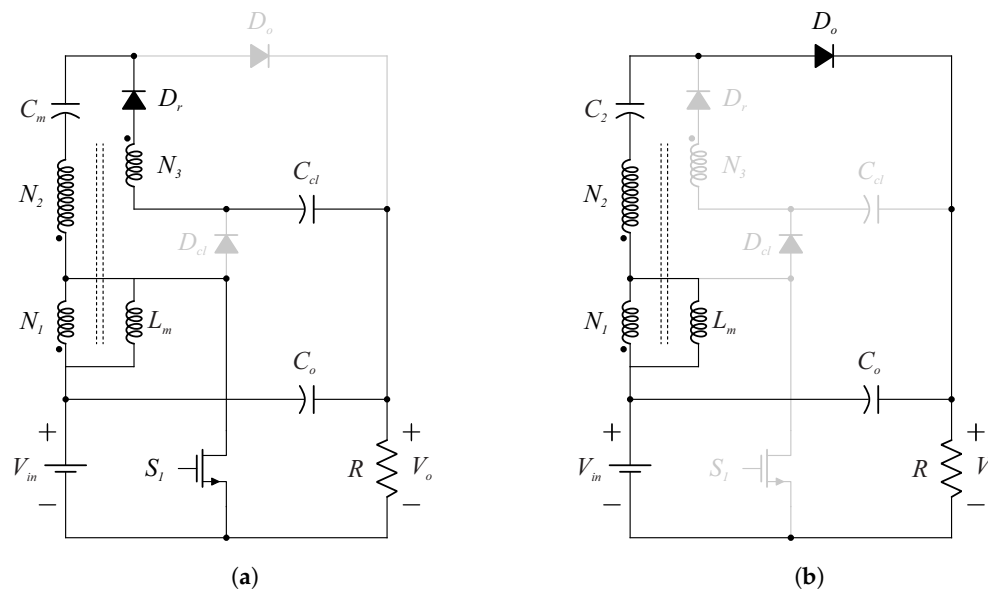

Figure 14. Main operation stages of the DC-DC converter proposed in [26]. (**a**) Operation stage that corresponds to the interval $[t_0 - t_1]$ of [26] (stage 1 of 3). (**b**) Operation stage that corresponds to the interval $[t_2 - t_3]$ of [26] (stage 3 of 3).

Furthermore, the reverse recovery problems of diodes D_o and D_r are attenuated by the leakage inductances associated with the windings N_2 and N_3 of the magnetic element, respectively. The energy stored in the leakage inductance of the primary winding is recovered to the load via the clamp circuit, which is formed by the diode D_{cl} and the capacitor C_{cl}. In addition to these features, the following characteristics of this converter should be observed: (i) very high input current ripple; (ii) hard switching at the turn-on

and turn-off transition of the switch; (iii) optimized magnetic design; (iv) common ground; and (v) it employs one switch and one magnetic core.

4.5. DC-DC Converter with Coupled Inductor and Switched Capacitor Proposed

The converter proposed in [27] integrates the coupled inductor and switched-capacitor techniques in modular units comprising of two capacitors, two diodes and one winding that is magnetically-coupled with the input inductor. In this way, the structure of this converter can be expanded to obtain high voltage gain. However, one should note that additional windings increase the cost and complexity of the converter.

In this topology, the leakage inductance of the secondary winding is used together with the capacitor C_m to create resonant stages. Thus, the currents flowing through the diodes, D_1 and D_2, decrease to zero before they became reverse-biased. As consequence, there are no losses caused by the reverse recovery of the diodes.

In a switching cycle, four different operation stages can be seen in this DC-DC converter. However, in order to observe the energy storage elements being charged and the power branch, one can evaluate only the first and third operation stages (Figure 15a,b). From this evaluation, one can see that:

- During the operation stage presented in Figure 15a, the coupled inductor is charged by the input voltage source. The energy stored in the clamp capacitor, C_{cl}, is transferred through the diode D_1 to the switched capacitor C_m, which is charged with a voltage equal to the sum of the voltages across the capacitor C_{cl} ($V_{C_{cl}} = \frac{V_{in}}{1-D}$) and across the windings N_1 and N_2 ($V_{N_1} = V_{in}$ and $V_{N_2} = \frac{N_2}{N_1} V_{in}$);
- During the operation stage shown in Figure 15b, the output diode conducts (D_2). When this happens, the voltage across the primary winding N_1 becomes equal to $\frac{D}{1-D} V_{in}$. Consequently, the voltage across N_2 is given by:

$$V_{N_2} = \frac{N_2}{N_1} \frac{D}{1-D} V_{in}. \tag{6}$$

In addition, the capacitor C_1 is charged by the sum of the voltage across N_2 and the voltage across the capacitor C_m. The power branch contains, associated in series, the following components: (i) the input voltage source; (ii) both windings of the coupled inductor; and (iii) the switching capacitor.
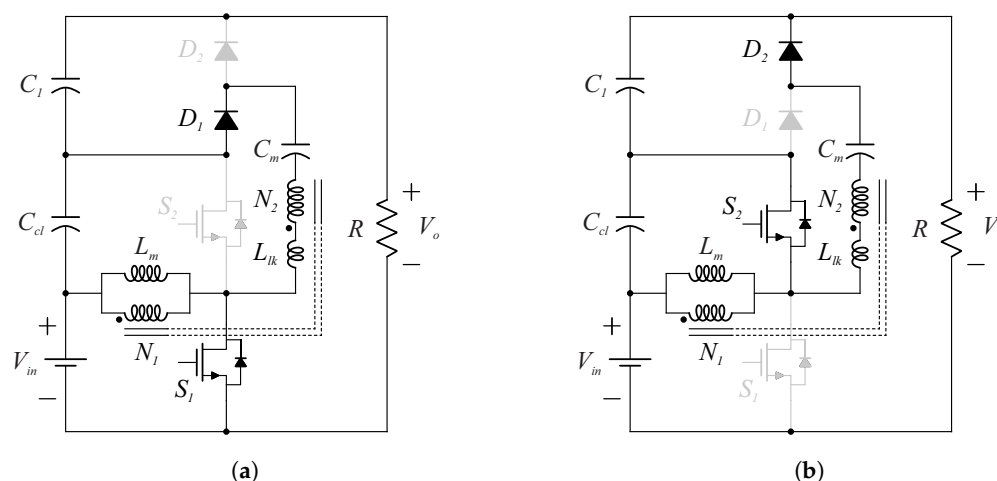

(a)   (b)

Figure 15. Main operation stages of the DC-DC converter proposed in [27]. (**a**) Operation stage that corresponds to the interval $[t_0 - t_1]$ of [27] (stage 1 of 4). (**b**) Operation stage that corresponds to the interval $[t_2 - t_3]$ of [27] (stage 3 of 4).

It is worth noting that the switch S_2 does not provide ZVS condition for switch S_1, even thought this converter features such capability. Considering this, it can be pointed out

that the DC-DC converter proposed in [27] has the following features: (i) hard switching at the turn-on and turn-off transition of the main switch; (ii) ZCS of the diodes; (iii) very high input current ripple; (iv) the input and output terminals share a common ground; (v) and it employs two switches and one magnetic core.

4.6. DC-DC Converter with Low and Steady Switch Voltage Stress Proposed

Similar to the converter presented in Section 4.5, the topology proposed in [28], shown in Figure 16, integrates the coupled inductor and switched capacitor techniques in a modular cell containing two capacitors and two diodes, but without windings magnetically-coupled with the input inductor. Thus, this converter can be vertically expanded in order to obtain a higher voltage gain without adding additional magnetic elements or windings.
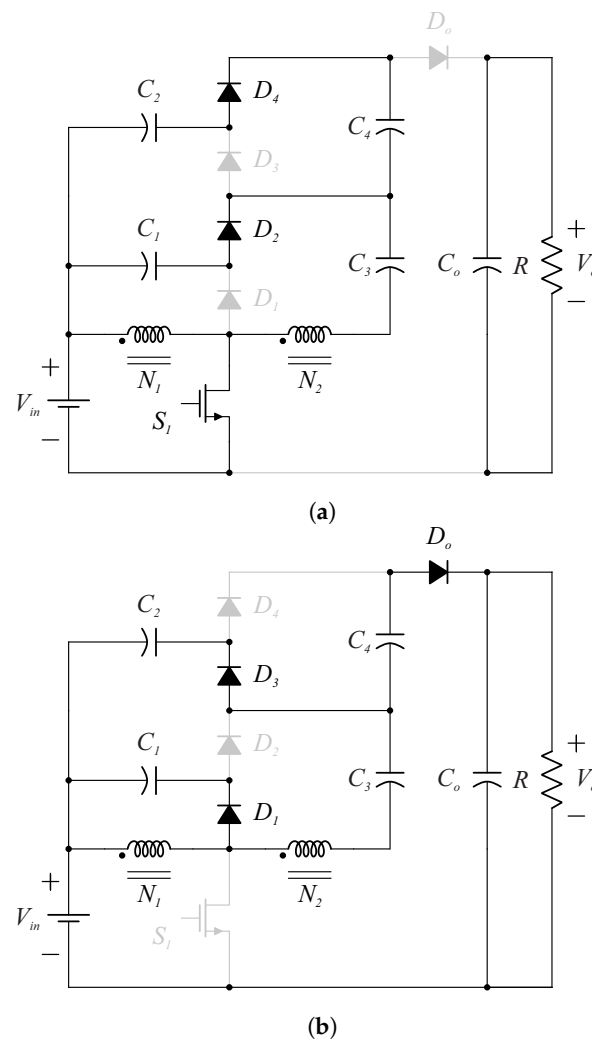

(a)

(b)

Figure 16. Main operation stages of the DC-DC converter proposed in [28]. (**a**) Operation stage that corresponds to the interval $[t_1 - t_2]$ of [28] (stage 2 of 4). (**b**) Operation stage that corresponds to the interval $[t_3 - t_4]$ of [28] (4 of 4).

In a switching cycle, this converter presents four different operation stages. However, the two stages illustrated in Figure 16a,b are sufficient to evaluate the energy storage elements being charged and the power branch. As a matter of fact, when evaluating these stages, it can be seen that:

- During the operation stage shown in Figure 16a, the coupled inductor is charged by the input voltage source. The energy stored in the capacitors C_1 and C_2 is transferred to the switched capacitors, C_3 and C_4, respectively. The voltage across the capacitor

C_3 is equal to the sum of the voltages across the capacitor C_1 ($V_{C_1} = \frac{V_{in}}{1-D}$) and across the windings N_1 and N_2 ($V_{N_1} = V_{in}$ and $V_{N_2} = \frac{N_2}{N_1} V_{in}$);

- During the operation stage illustrated in Figure 16b, the output diode, D_o, conducts. While this happens, the voltage across the primary winding N_1 is equal to $\frac{D}{1-D} V_{in}$. Consequently, the voltage across N_2 is given by:

$$V_{N_2} = \frac{N_2}{N_1} \frac{D}{1-D} V_{in}. \tag{7}$$

The capacitor C_2 is charged by the voltage across the windings of the coupled inductor added to the voltage across the capacitor C_3. The power branch contains, associated in series, the following components: (i) the input voltage source; (ii) both windings of the coupled inductor; and (iii) the two switching capacitors.

Even thought there are no resonant operation stages, the diodes are turned off with ZCS. Then, briefly, the main features of this converter are: (i) hard switching at the turn-on and turn-off transition of the switch; (ii) ZCS of the diodes; (iii) very high input current ripple; (iv) common ground; and (v) it employs one switch and one magnetic core.

4.7. Hybrid Transformer DC-DC Converter with Optimized Magnetics Proposed

In 2015, Gu et al. [29] proposed a DC-DC converter based on a flyback topology with a coupled inductor instead of the normal transformer, as shown in Figure 17. From the basic structure of the flyback converter, Gu et al. (2015) added to this topology: (i) an active clamp circuit; (ii) a connection between input and output common terminals; and (iii) the capacitor C_m and the diode D_r. The two-winding magnetic element operates as both coupled inductor and transformer, which optimizes its use. Besides that, the magnetizing current is bidirectional, so its average value can be purposefully reduced to allow designs with small magnetizing inductance. As consequence, the number of turns of the windings is reduced, which implies lower conduction losses and enables the use of magnetic cores with small dimensions.

The gate signals of S_1 and S_2 are complementary. A dead time is added to ensure the charging and discharging of the leakage capacitances of the switches. As a matter of fact, this is one of the necessary conditions for the switches to be turned on with zero-voltage switching.

During a switching cycle, the DC-DC converter proposed in [29] presents eight different operation stages. However, the stages shown in Figure 17a,b are sufficient to observe the energy storage elements being charged and the power branch. Based on these stages, the following characteristics can be seen:

- During the operation stage presented in Figure 17a, the magnetizing inductance is charged by the input voltage source. The energy stored in the capacitors C_{cl} is transferred to the switched capacitor, C_m, via the regenerative diode, D_r. The voltage across the capacitor C_m is equal to the sum of the voltages across the capacitor C_{cl} ($V_{C_{cl}} = \frac{V_{in}}{1-D}$) and across the windings N_1 and N_2 ($V_{N_1} = V_{in}$ and $V_{N_2} = \frac{N_2}{N_1} V_{in}$, respectively). It should be noted that the loop formed by C_m, C_r, D_r, N_2 and L_{lk} creates a resonance stage.
- During the operation stage shown in Figure 17b, the output diode, D_o, conducts. At this moment, the voltage across the primary winding N_1 is equal to $\frac{D}{1-D} V_{in}$. Consequently, the voltage across N_2 is given by:

$$V_{N_2} = \frac{N_2}{N_1} \frac{D}{1-D} V_{in}. \tag{8}$$

The power branch contains, associated in series: (i) the input voltage source; (ii) the two magnetic windings and the switching capacitor. As in the stage presented in the previous item, there is a resonant loop formed by C_m, C_r, D_o, R, N_2 and L_{lk}.

The operation stages described above are finished when the resonant currents flowing through the diodes naturally decreases to zero. Thus, there are no losses caused by reverse recovery of the diodes. Also, although it is not shown in Figure 17a,b, the switches are commanded to conduct when the current begins to flow through their free wheeling diode, which means that they are turned on with zero-voltage switching. Therefore, the main features of this converter are: (i) ZVS turn-on of the switches and ZCS of the diodes; (ii) very high input current ripple; (iii) common ground; and (iv) it employs two switches and one magnetic core.
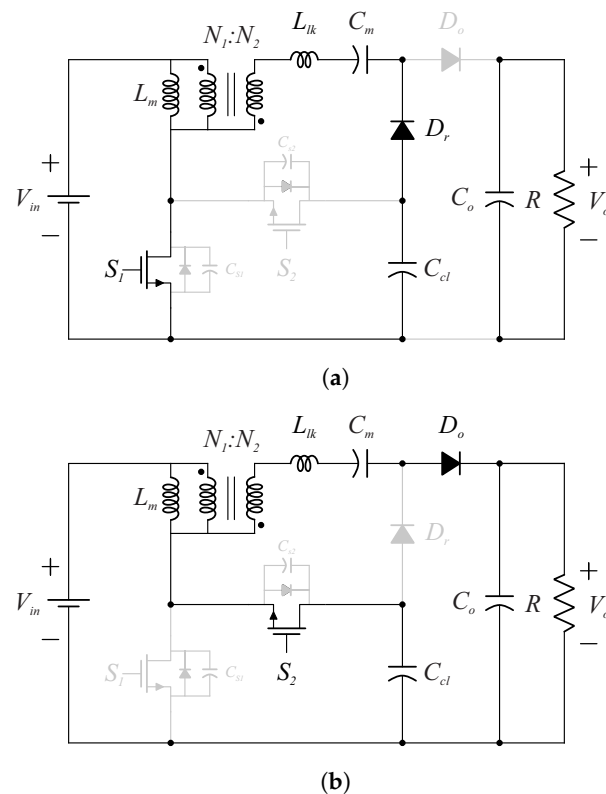

(**a**)

(**b**)

Figure 17. Main operation stages of the DC-DC converter proposed in [29]. (**a**) Operation stage that corresponds to the interval $[t_2 - t_3]$ of [29] (3 of 8). (**b**) Operation stage that corresponds to the interval $[t_6 - t_7]$ of [29] (7 of 8).

4.8. Step-Up Interleaved DC-DC Converter with Coupled Inductor and Built-In Transformer Voltage Multiplier Cell Proposed

The interleaved DC-DC converter proposed in [30], shown in Figure 18, employs a VMC based on magnetic coupling and switched capacitor techniques. The submodules of this topology are similar to the converter proposed in [23] (already presented in Section 4.1), however, here, Nouri et al. (2019) [30] replaces the input inductor of each submodule by a coupled inductor and integrates its secondary winding in the power branch. If this modification were made in the converter without interleaved input, the low input current ripple characteristic would be compromised. In the interleaved topology, the currents flowing through the primary windings of the coupled inductors are displaced by 180°, so that, when summed, there is a cancellation of the current ripple, yielding in a continuous input current.

It should be noted that Nouri et al. (2019) [30] connects the two submodules through the primary winding of the built-in transformer, so that, when the output diode of one of the submodules conducts, the voltage across its primary winding becomes equal to the output voltage of the traditional boost converter. Consequently, the voltage across the secondary winding reaches high values even if a low turns ratio transformer is used.
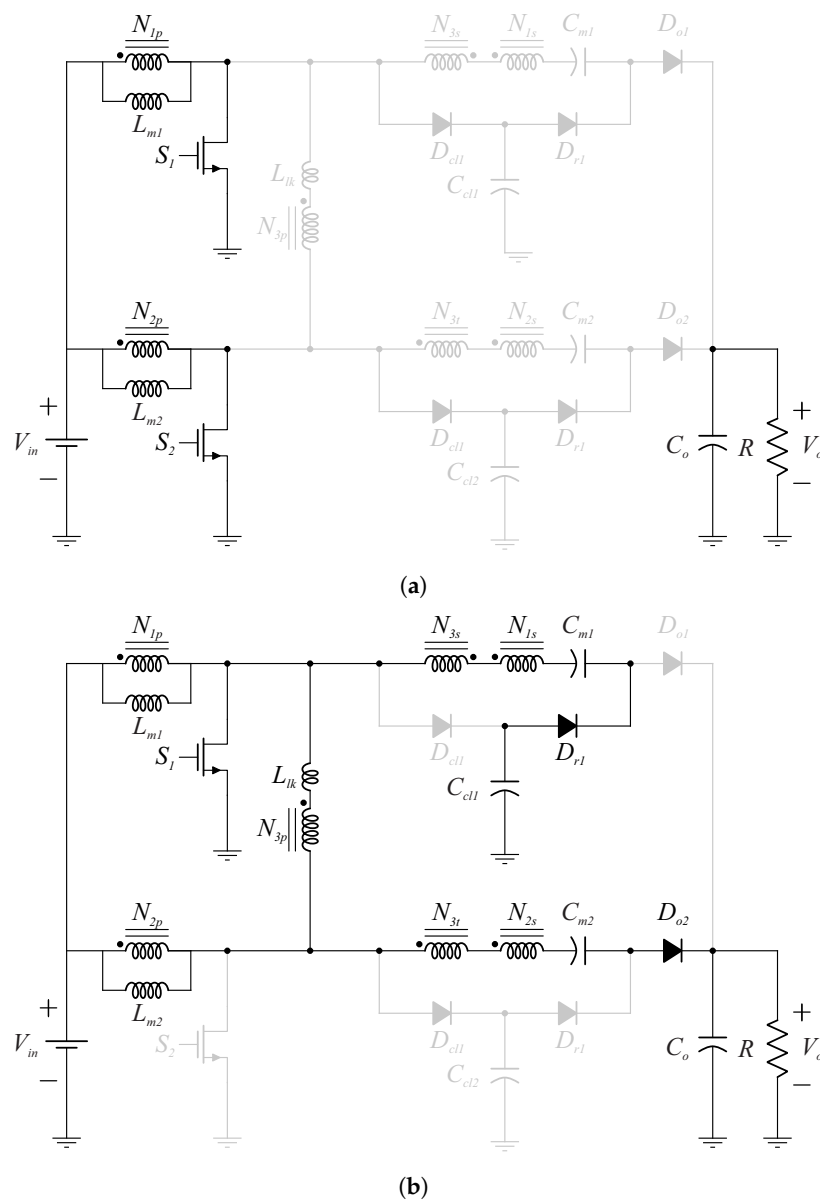
(**a**)

(**b**)

Figure 18. Main operation stages of the step-up interleaved DC-DC converter proposed in [30]. (**a**) Operation stage that corresponds to the interval $[t_0 - t_1]$ of [30] (1 of 12). (**b**) Operation stage that corresponds to the interval $[t_4 - t_5]$ of [30] (5 of 12).

During a switching cycle, this converter has twelve operation stages, in which six of them are symmetrical to each other. However, the stages illustrated in Figure 18a,b are sufficient to evaluate the energy storage elements being charged and the power branch, which contains, associated in series, the energy storage elements and the high voltage windings of the magnetic elements. More details about the operation stages presented in Figure 18 are presented below:

- During the interval in which both switches are conducting, represented in Figure 18a, the coupled inductors are charged by the input voltage;
- During the interval in which one of the switches remains turned off while the other conducts, represented in Figure 18b, the output diode of the bottom submodule conducts. The energy of the capacitor C_{cl1} is recycled to the switched capacitor C_{m1} via the regenerative diode D_{r1}. At this moment, the voltage across the primary winding of the transformer, N_{3p}, becomes equal to the voltage across the clamp capacitors (which is also equal to the output voltage of the conventional boost converter). As consequence, the voltage across N_{3t} is given by:

$$V_{N_{3t}} = \left(\frac{N_{3t}}{N_{3p}}\right)\frac{V_{in}}{1-D}.$$ (9)

The power branch contains the input voltage supply in series with both windings of the coupled inductors of the bottom submodule (N_{3t}) and C_{m2}.

In this topology, the reverse recovery of the diodes is mitigated due to the leakage inductance of the magnetic elements, which control the rate at which the current flowing through them decreases during their turn-off transition. Considering this, it can be pointed out that this converter features: (i) hard switching at the turn-on and turn-off transition of the switch; (ii) low input current ripple; (iii) high voltage gain with high degree of freedom; and (iv) it employs two switches and three magnetic cores.

4.9. Step-Up Interleaved DC-DC Converter with Dual Coupled Inductors Proposed

Differently from the converter presented in the previous subsection, the step-up interleaved DC-DC converter proposed in [31], shown in Figure 19, optimizes the number of components by sharing a single clamp capacitor, C_{cl}, for the two main switches, S_1 and S_2. As consequence, only one regenerative diode D_r is needed. Still, there is only one power branch and two magnetic cores.
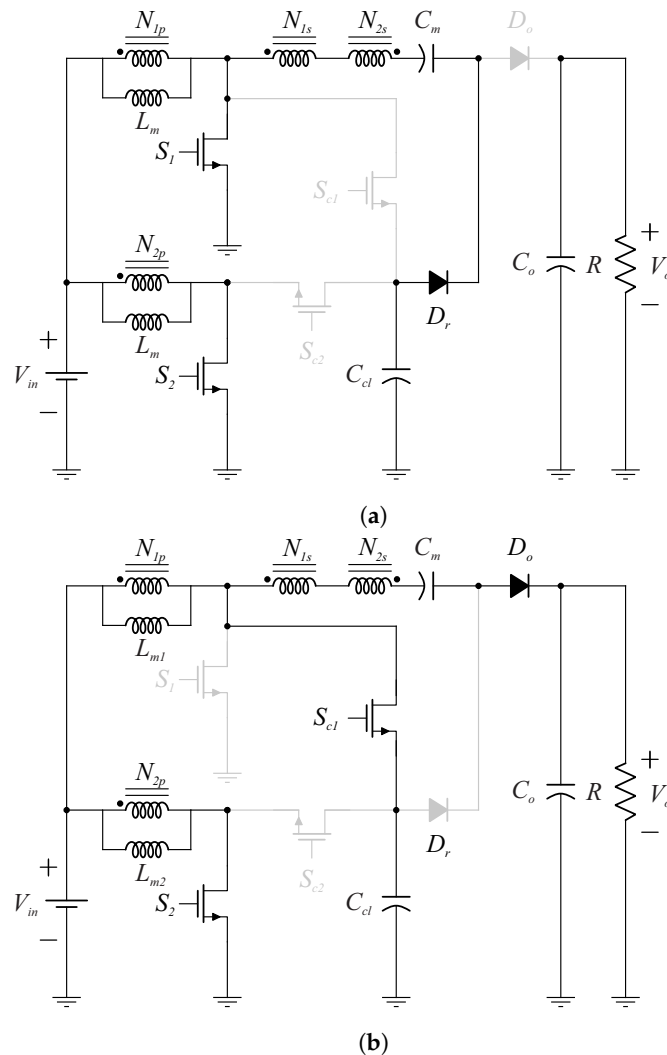
(a)

(b)

Figure 19. Main operation stages of the step-up interleaved DC-DC converter proposed in [31]. (a) Operation stage that corresponds to the interval $[t_1 - t_2]$ of [31] (2 of 14). (b) Operation stage that corresponds to the interval $[t_5 - t_6]$ of [31] (5 of 14).

In order to obtain ZVS of the main switches, the Forouzesh et al. (2018) [31] include two auxiliary switches (S_{c1} and S_{c2}) and turned them on at the moment that the currents are flowing through their free wheeling diodes (for simplicity purpose, this stage is not shown in the circuits in Figure 19).

In a switching cycle, it can be noted that this converter has fourteen operation stages. However, the operation stages shown in Figure 19a,b are sufficient to observe the energy storage elements being charged and the power branch, which contains, associated in series, the following components: the energy storage elements and the high voltage windings of the magnetic elements. Besides that, it should be noted that:

- During the interval in which both switches conduct, illustrated in Figure 19a, the coupled inductors are charged by the input voltage and the energy stored in the clamp capacitor, C_{cl}, is transferred to the switched capacitor, C_m, via the regenerative diode D_r;
- During the interval in which one of the switches remains turned off and the other are conducting, as shown in Figure 19b, the output diode conducts. In this stage, the voltage across the primary winding N_{1p} is equal to the difference between the voltages across the clamp capacitors (which is equal to the output voltage of the conventional boost converter) and the input voltage. As consequence, the voltage across N_{1s} is given by:

$$V_{N_{1s}} = \left(\frac{N_{1s}}{N_{1p}} \right) \frac{D}{1 - D} V_{in}. \tag{10}$$

The power branch contains the clamp capacitor in series with both windings of the coupled inductor and C_m.

It is not difficult to see that, when compared to the interleaved topology presented in [30], this converter has lower voltage gain. This happens because the voltages across the secondary windings of the power branch are given by $V_{N_{1s}} = \frac{N_{1s}}{N_{1p}} \frac{D}{1-D} V_{in}$ and $V_{N_{2s}} = \frac{N_{2s}}{N_{2p}} V_{in}$. On the other hand, the voltage stresses on the diodes in this converter are smaller than the voltage stresses in Nouri et al.'s solution [30].

Although there are no resonant stages, the diodes are turned off with ZCS. In addition, this converter features: (i) ZVS turn-on of the switches; (ii) low input curren ripple; (iii) high voltage gain with high degree of freedom; and (iv) it employs four switches and two magnetic cores.

## 5. Circuit Performance Comparison and Evaluation

Table 2 presents the main circuit features of the explained previously published switched-capacitor and coupled-inductor based converters. Although not shown, all converters in Table 2 are common grounded. Figure 20 shows line charts of the voltage gain, normalized maximum voltage stresses across diodes and switches, and measured efficiency of the converters presented in Table 2 under the same conditions (the total turn ratios was kept the same for all converters, i.e, for three-windings coupled-inductors and built-in transformer based converters $n = 2$, $m = 2$, and for two-windings coupled-inductors and built-in transformer based converters $n = 4$).

Figure 20a depicts the voltage gain comparison results. It can been noted that all the converters presented can meet the high voltage gain requirement for DC-DC stage in MICs (e.g., 45 V-input to 400 V-output) without operating at extreme duty cycle. The converter presented in [26] has the lowest voltage gain capability even employing a three-winding coupled inductor. The reason for this is that, in this converter, the third winding should not be designed to increase the voltage gain, but instead to decrease the RMS value of the currents flowing through the semiconductors.
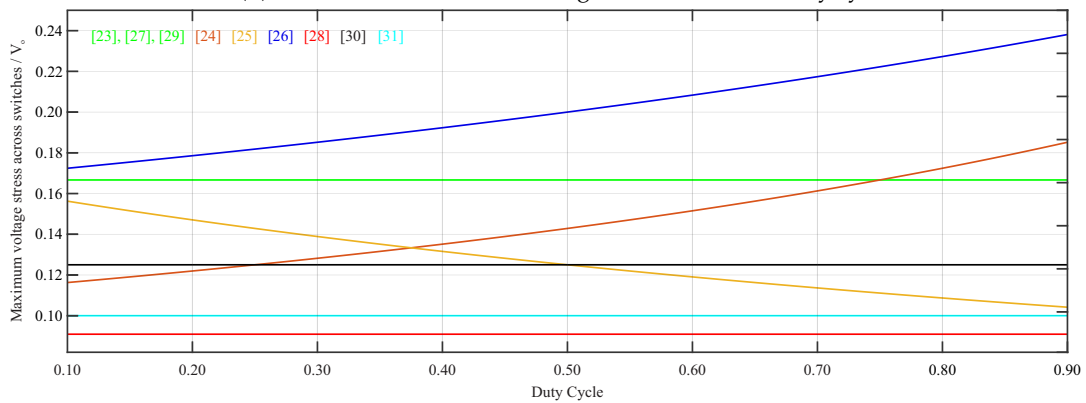
From Figure 20b, it can been observed that the converter presented in [28] has the lowest voltage across diodes. Such feature alongside ZCS turn-off minimize the diode conduction and reverse recovery losses.
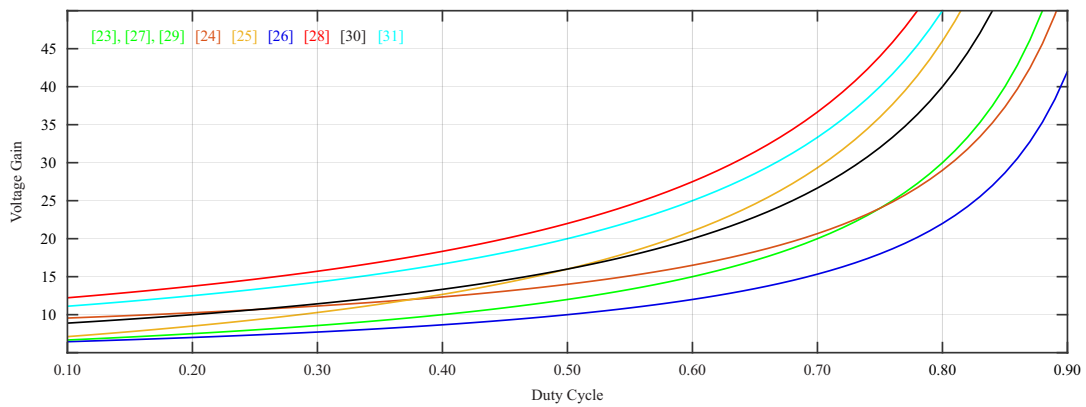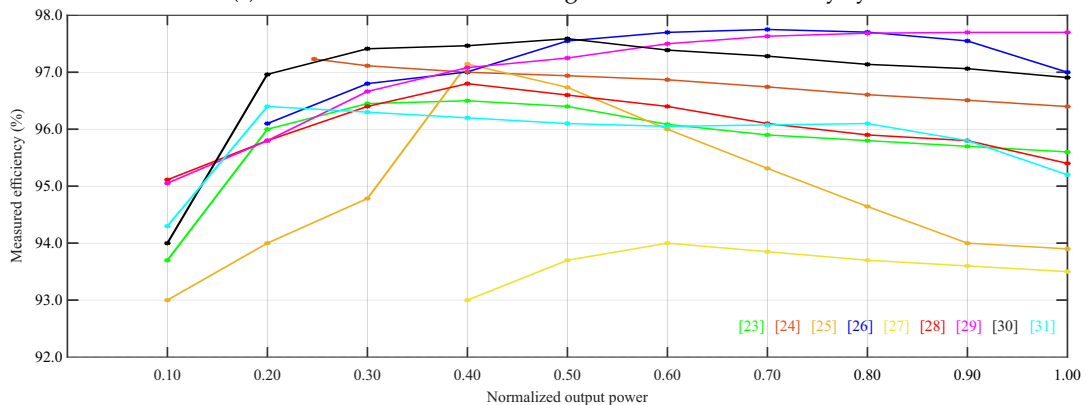
(**a**) Voltage gain X Duty cycle.
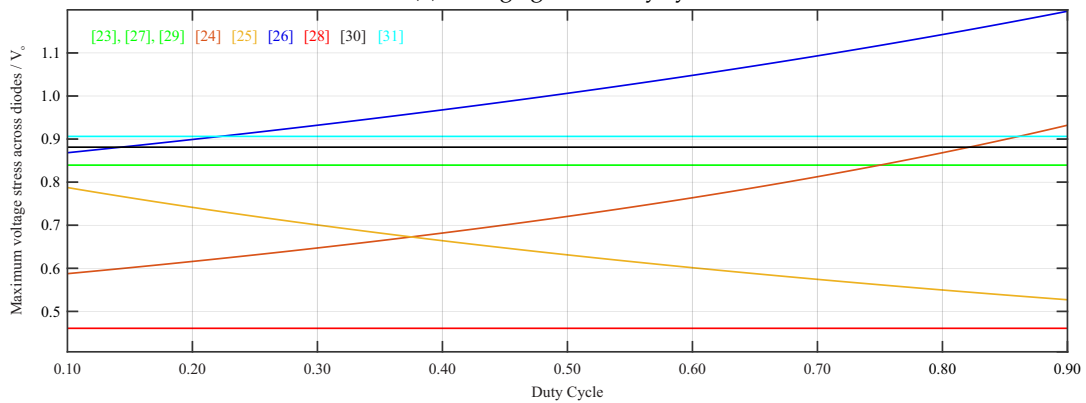
(**b**) Normalized maximum voltage across diodes X Duty cycle.

(**c**) Normalized maximum voltage across switches X Duty cycle.

(**d**) Measured efficiency X Normalized output power.

Figure 20. Comparison between the previously presented converters: (**a**) voltage gain; (**b**) normalized maximum voltage across diodes; (**c**) normalized maximum voltage across switches; and (**d**) measured efficiency.

Table 2. Main characteristics of the previously presented switched-capacitor coupled-inductor based converters.

Converters	Voltage Gain	Max. Voltage across Switches	Max. Voltage across Diodes	Number of Components				Input Current Ripple	Soft Switching of Switches	Soft Switching of Diodes	Efficiency (Full Load)
				S	D	C	MC				
[23]	$\frac{2+n}{1-D}$	$\frac{V_o}{2+n}$	$\frac{(1+n)V_o}{2+n}$	1	3	3	2	Low	ZCS turn on QR turn off	ZCS *	95.6% 500 W
[24]	$\frac{1+n(1+D)}{1-D}$	$\frac{V_o}{1+n(1+D)}$	$\frac{nV_o}{1+n(1+D)}$	1	4	5	2	Low	ZCS turn on	ZCS	96.4% 200 W
[25]	$\frac{2+n(1+D)}{1-D}$	$\frac{V_o}{2+n(1+D)}$	$\frac{(1+n)V_o}{2+n(1+D)}$	1	4	4	1	High	Hard	ZCS *	≈94.0% 200 W
[26]	$\frac{2+n}{1-D} + m$	$\frac{V_o}{2+n+m(1-D)}$	$\frac{(1+n+m)V_o}{2+n+m(1-D)}$	1	3	3	1	High	Hard	-	≈97.0% 500 W
[27]	$\frac{2+n}{1-D}$	$\frac{V_o}{2+n}$	$\frac{(1+n)V_o}{2+n}$	2	2	3	1	High	Hard	ZCS	≈93.5% 200 W
[28]	$\frac{3+2n}{1-D}$	$\frac{V_o}{3+2n}$	$\frac{(1+n)V_o}{3+2n}$	1	5	5	1	High	Hard	ZCS	95.4% 300 W
[29]	$\frac{2+n}{1-D}$	$\frac{V_o}{2+n}$	$\frac{(1+n)V_o}{2+n}$	2	2	3	1	High	ZVS turn on	ZCS	97.7% 250 W
[30]	$\frac{2(N+1)+n}{1-D}$	$\frac{V_o}{2(N+1)+n}$	$\frac{(2N+1+n)V_o}{2(N+1)+n}$	2	6	5	3	Very low	Hard	-	96.9% 1.3 kW
[31]	$\frac{2(n+1)}{1-D}$	$\frac{V_o}{2(n+1)}$	$\frac{(2n+1)V_o}{2(n+1)}$	4	2	3	2	Very low	ZVS turn on	ZCS	95.2% 1 kW

S.: Switches; D.: Diodes; C.: Capacitors; M.C.: Magnetic Cores; *: except output diode. The total turns ratio have been kept the same for all topologies.

From Figure 20c, it can been seen that the maximum voltage across the switches for most of the presented converters correspond to 10% e 20% of the output voltage, allowing for employing MOSFET with low $R_{DS,on}$.

It must been noted that the converters with the highest voltage gain capability employ the greatest number of components, and the higher the voltage gain, the lower the voltage across the switches, which leads to reduce the switch conduction losses and hence to achieve high efficiency even for hard switching operation.

In order to achieve ZVS for the switches, the converters proposed in [29,31] employ an auxiliary switch. The converters proposed in [23,24] feature just one power switch and perform ZCS for the switch at its turn-on instant. However, ZVS for the switches impacts more on improving the efficiency of converters that employ MOSFET than ZCS for the switches. Also, either an input filter inductor or interleaved technique should be used to reduce the input current ripple. This benefits the input sources such as PV module and decreases the input current RMS value and hence conduction losses.

In order to evaluate the possibility of using these DC-DC converters as first power conversion stage on commercial solutions, let us consider the two-stage MIC from Texas Instruments (TI) presented in [5] (Figure 21). From Figure 21, one can observe that the DC-DC converter employed by the TI's microinverter topology is an isolated flyback converter with active clamped and voltage multiplier cell.
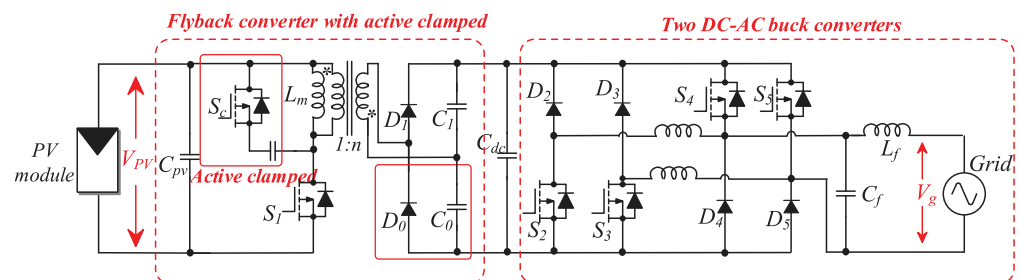

Figure 21. Commercial two-stage MIC from Texas Instruments—TI 280W [5].

The DC-DC converter shown in Figure 17 was derived from the active-clamp flyback converter as well, and such as it features ZVS for both switches and high input current

ripple. In addition, this topology is common ground. This brings up another important advantage related to the leakage current problems.

Regarding components amount, both converters employ the same number of capacitors (C_{pv} shown in Figure 21 must also be employed in the converter shown in Figure 17 due to its high input current ripple), diodes, magnetic cores and switches—respectively: 3, 2, 1 and 2. Thus, if galvanic isolation is not mandatory, the topology presented in [29] can be used as first power conversion stage in MICs.

6. Conclusions

Using the categorization of DC-DC converters approached in this paper, it can be said that the characteristics needed to meet the requirements of PV applications such as solar optimizers or PV microinverters, beyond the high voltage gain, are: non-isolated and common ground, unidirectional and current fed. Besides, soft switching and resonant mechanisms can lead to reduced switching loss. Furthermore, the DC-DC converters based on switched capacitor and magnetic coupling listed and discussed in this paper show that:

- to provide high voltage gain, it is sufficient to employ just one switch (combined with energy storage elements);
- ZVS for the switches is obtained by using an auxiliary switch;
- to achieve ZCS for the diodes, the converter does not necessarily have resonant stages;
- to feature low input current ripple, one must employ either input filter inductor or interleaved technique.

It should be noted that the inputs of the DC-DC converters presented throughout this paper contain a voltage source (V_{in}) in series with a magnetizing inductance. As a result, the voltage stress on the main switch is equal to $\frac{D}{1-D}V_{in}$, where D is the duty cycle.

Abbreviations

The following abbreviations are used in this manuscript:

BRF	Below resonant frequency
MIC	Module integrated converter
MPPT	Maximum power point tracking
ORF	Over resonant frequency
PV	Photovoltaic
QR	Quasi-resonant
TI	Texas Instruments
VMC	Voltage multiplier cell
ZCS	Zero current switching
ZVS	Zero voltage switching

References

1. IRENA. *Future of Solar Photovoltaic: Deployment, Investment, Technology, Grid Integration and Socio-Economic Aspects*; Technical Report; A Global Energy Transformation: Paper; International Renewable Energy Agency—IRENA: Abu Dhabi, United Arab Emirates, 2019.
2. Romero-Cadaval, E.; Spagnuolo, G.; Franquelo, L.G.; Ramos-Paja, C.A.; Suntio, T.; Xiao, W.M. Grid-Connected Photovoltaic Generation Plants: Components and Operation. *IEEE Ind. Electron. Mag.* **2013**, *7*, 6–20. [CrossRef]
3. Kouro, S.; Leon, J.I.; Vinnikov, D.; Franquelo, L.G. Grid-Connected Photovoltaic Systems: An Overview of Recent Research and Emerging PV Converter Technology. *IEEE Ind. Electron. Mag.* **2015**, *9*, 47–61. [CrossRef]
4. Santos de Carvalho, M.R.; Bradaschia, F.; Rodrigues Limongi, L.; de Souza Azevedo, G.M. Modeling and Control Design of the Symmetrical Interleaved Coupled-Inductor-Based Boost DC-DC Converter with Clamp Circuits. *Energies* **2019**, *12*, 3432. [CrossRef]
5. Yuan, J.; Blaabjerg, F.; Yang, Y.; Sangwongwanich, A.; Shen, Y. An Overview of Photovoltaic Microinverters: Topology, Efficiency, and Reliability. In Proceedings of the 2019 IEEE 13th International Conference on Compatibility, Power Electronics and Power Engineering (CPE-POWERENG), Sonderborg, Denmark, 23–25 April 2019; pp. 1–6. [CrossRef]
6. Pereira, A.V.C.; Cavalcanti, M.C.; Azevedo, G.M.; Bradaschia, F.; Neto, R.C.; Carvalho, M.R.S.d. A Novel Single-Switch High Step-Up DC–DC Converter with Three-Winding Coupled Inductor. *Energies* **2021**, *14*, 6288. [CrossRef]
7. Zhang, X.; Zhao, T.; Mao, W.; Tan, D.; Chang, L. Multilevel Inverters for Grid-Connected Photovoltaic Applications: Examining Emerging Trends. *IEEE Power Electron. Mag.* **2018**, *5*, 32–41. [CrossRef]
8. Forouzesh, M.; Siwakoti, Y.P.; Gorji, S.A.; Blaabjerg, F.; Lehman, B. Step-Up DC–DC Converters: A Comprehensive Review of Voltage-Boosting Techniques, Topologies, and Applications. *IEEE Trans. Power Electron.* **2017**, *32*, 9143–9178. [CrossRef]
9. Starzyk, J.; Jan, Y.W.; Qiu, F. A DC-DC charge pump design based on voltage doublers. *IEEE Trans. Circuits Syst. I Fundam. Theory Appl.* **2001**, *48*, 350–359. [CrossRef]
10. Sri Revathi, B.; Prabhakar, M. Non isolated high gain DC-DC converter topologies for PV applications—A comprehensive review. *Renew. Sustain. Energy Rev.* **2016**, *66*, 920–933. [CrossRef]
11. Jiao, Y.; Luo, F.; Zhu, M. Voltage-lift-type switched-inductor cells for enhancing DC-DC boost ability: Principles and integrations in Luo converter. *Power Electron. IET* **2011**, *4*, 131–142. [CrossRef]
12. Axelrod, B.; Berkovich, Y.; Ioinovici, A. Switched-Capacitor/Switched-Inductor Structures for Getting Transformerless Hybrid DC–DC PWM Converters. *IEEE Trans. Circuits Syst. I Regul. Pap.* **2008**, *55*, 687–696. [CrossRef]
13. Yang, L.S.; Liang, T.J.; Chen, J.F. Transformerless DC–DC Converters with High Step-Up Voltage Gain. *IEEE Trans. Ind. Electron.* **2009**, *56*, 3144–3152. [CrossRef]
14. Liu, H.C.; Li, F. Novel High Step-Up DC–DC Converter with an Active Coupled-Inductor Network for a Sustainable Energy System. *IEEE Trans. Power Electron.* **2015**, *30*, 6476–6482. [CrossRef]
15. Tang, Y.; Fu, D.; Wang, T.; Xu, Z. Analysis of Active-Network Converter with Coupled Inductors. *IEEE Trans. Power Electron.* **2015**, *30*, 4874–4882. [CrossRef]
16. Tang, Y.; Fu, D.; Wang, T.; Xu, Z. Hybrid Switched-Inductor Converters for High Step-Up Conversion. *IEEE Trans. Ind. Electron.* **2015**, *62*, 1480–1490. [CrossRef]
17. Mulani, K.A.; Shewale, A.J.; Pawar, S.H. Integrated interleaved fly-back converter for standalone PV application. In Proceedings of the 2017 International Conference on Intelligent Sustainable Systems (ICISS), Palladam, India, 7–8 December 2017; pp. 751–755.
18. Witulski, A. Introduction to modeling of transformers and coupled inductors. *IEEE Trans. Power Electron.* **1995**, *10*, 349–357. [CrossRef]
19. Prudente, M.; Pfitscher, L.L.; Emmendoerfer, G.; Romaneli, E.F.; Gules, R. Voltage Multiplier Cells Applied to Non-Isolated DC–DC Converters. *IEEE Trans. Power Electron.* **2008**, *23*, 871–887. [CrossRef]
20. Ismail, E.H.; Al-Saffar, M.A.; Sabzali, A.J.; Fardoun, A.A. A Family of Single-Switch PWM Converters with High Step-Up Conversion Ratio. *IEEE Trans. Circuits Syst. I Regul. Pap.* **2008**, *55*, 1159–1171. [CrossRef]
21. Fardoun, A.A.; Ismail, E.H. Ultra Step-Up DC–DC Converter with Reduced Switch Stress. *IEEE Trans. Ind. Appl.* **2010**, *46*, 2025–2034. [CrossRef]
22. Prudente, M.; Pfitscher, L.; Gules, R. A Boost Converter with Voltage Multiplier Cells. In Proceedings of the 2005 IEEE 36th Power Electronics Specialists Conference, Dresden, Germany, 16 June 2005; pp. 2716–2721.
23. Deng, Y.; Rong, Q.; Li, W.; Zhao, Y.; Shi, J.; He, X. Single-Switch High Step-Up Converters with Built-In Transformer Voltage Multiplier Cell. *IEEE Trans. Power Electron.* **2012**, *27*, 3557–3567. [CrossRef]
24. Forouzesh, M.; Yari, K.; Baghramian, A.; Hasanpour, S. Single-switch high step-up converter based on coupled inductor and switched capacitor techniques with quasi-resonant operation. *IET Power Electron.* **2017**, *10*, 240–250. [CrossRef]
25. Ai, J.; Lin, M. Ultralarge Gain Step-Up Coupled-Inductor DC–DC Converter with an Asymmetric Voltage Multiplier Network for a Sustainable Energy System. *IEEE Trans. Power Electron.* **2017**, *32*, 6896–6903. [CrossRef]
26. Siwakoti, Y.P.; Blaabjerg, F. Single Switch Nonisolated Ultra-Step-Up DC–DC Converter with an Integrated Coupled Inductor for High Boost Applications. *IEEE Trans. Power Electron.* **2017**, *32*, 8544–8558. [CrossRef]
27. Ye, Y.; Cheng, K.W.E.; Chen, S. A High Step-up PWM DC-DC Converter with Coupled-Inductor and Resonant Switched-Capacitor. *IEEE Trans. Power Electron.* **2017**, *32*, 7739–7749. [CrossRef]

28. Hassan, W.; Lu, D.D.C.; Xiao, W. Single-Switch High Step-Up DC–DC Converter with Low and Steady Switch Voltage Stress. *IEEE Trans. Ind. Electron.* **2019**, *66*, 9326–9338. [CrossRef]

29. Gu, B.; Dominic, J.; Chen, B.; Zhang, L.; Lai, J.S. Hybrid Transformer ZVS/ZCS DC–DC Converter with Optimized Magnetics and Improved Power Devices Utilization for Photovoltaic Module Applications. *IEEE Trans. Power Electron.* **2015**, *30*, 2127–2136. [CrossRef]

30. Nouri, T.; Vosoughi, N.; Hosseini, S.H.; Babaei, E.; Sabahi, M. An Interleaved High Step-Up Converter with Coupled Inductor and Built-In Transformer Voltage Multiplier Cell Techniques. *IEEE Trans. Ind. Electron.* **2019**, *66*, 1894–1905. [CrossRef]

31. Forouzesh, M.; Shen, Y.; Yari, K.; Siwakoti, Y.P.; Blaabjerg, F. High-Efficiency High Step-Up DC–DC Converter with Dual Coupled Inductors for Grid-Connected Photovoltaic Systems. *IEEE Trans. Power Electron.* **2018**, *33*, 5967–5982. [CrossRef]